Force Fields for "Ultrafast" Photochemistry: The S_2 ($1B_u$) → S_1 ($2A_g$) → S_0 ($1A_g$) Reaction Path for *all-trans*-Hexa-1,3,5-triene

Marco Garavelli,[†] Paolo Celani,[‡] Fernando Bernardi,[†] Michael A. Robb,*[,‡] and Massimo Olivucci*[,†]

Contribution from the Dipartimento di Chimica "G. Ciamician", Università di Bologna, Via Selmi 2, 40126 Bologna, Italy, and King's College London, London WC2R 2LS, United Kingdom

Received April 22, 1997. Revised Manuscript Received September 2, 1997[⊗]

Abstract: High-level *ab initio* quantum chemical computations (MC-SCF and multireference Møller−Plesset perturbation theory) have been used to investigate the *composite* relaxation path on three different singlet electronic states of an isolated *all-trans*-hexa-1,3,5-triene (*trans*-HT) molecule: the spectroscopic B_u (valence-ionic) state, the lower lying dark (i.e. symmetry forbidden covalent) $2A_g$ state (S_1), and finally the ground state (S_0). Our results support the hypothesis that IVR (*internal vibrational energy redistribution*) from totally symmetric to non-totally symmetric modes must control the dynamics of ultrafast decay in short *all-trans* polyenes. The salient features of the reaction path are as follows: (a) Motion out of the S_2 **FC** region and the subsequent relaxation along the S_1 energy surface lies within the space of *totally symmetric* deformations of the *trans*-HT molecular backbone. (b) The triggering of fast $S_1 \rightarrow S_0$ radiationless decay requires a *non-totally symmetric* deformation of the molecular backbone along a nearly barrierless (±2 kcal mol^{-1}) path. (c) The molecular structure at the $S_1 \rightarrow S_0$ decay channel (i.e. at the S_1/S_0 crossing point) and its subsequent evolution on the relaxation path which develops along the S_0 energy surface indicate that reactant back-formation must be the favored process.

1. Introduction

Ultrafast (i.e., femtosecond) photochemical processes are the subject of intensive experimental research.[1] The development of ultrashort laser pulses has made it possible to follow the time evolution of fast photoinduced processes, including excited state relaxation and chemical reactions.[2] These experimental methods are increasing our general knowledge of the "primary events" which control the final outcome of the absorption of a photon. Here, the results of experiments carried out on small organic molecules which undergo simple intramolecular transformations are particularly valuable because the interplay of theory (*ab initio* electronic structure computations) and experiment is fruitful. Short polyenes like buta-1,3-dienes, hexa-1,3,5-trienes, and octa-1,3,5,7-tetraenes are small molecules which undergo photochemical *cis*−*trans* isomerization.[3] Time-resolved studies on such polyenes are of fundamental importance in photochemistry because they unveil the changes in bonding and molecular structure occurring immediately after the excited state is generated and the way in which these changes provide the driving force for the generation of the photoproducts.

Very recently, considerable effort has been devoted to the investigation of linear hexa-1,3,5-trienes in an attempt to understand their ultrafast excited state dynamics.[4−8] In these experiments a polyene molecule is typically promoted to its spectroscopic (i.e., symmetry allowed) $1B_u$ state (S_2). The photoexcitation initiates a radiationless relaxation process which must involve a trajectory that evolves, sequentially, on three different singlet electronic states: the spectroscopic $1B_u$ state, the lower lying dark (i.e., symmetry forbidden) $2A_g$ state (S_1), and finally the ground state (S_0). Making use of different time-resolved spectroscopic methodologies the time constants for the radiationless deactivation of *tZt*-hexa-1,3,5-triene[4,5,6] (*cis*-HT) and *all-trans*-hexa-1,3,5-triene (*trans*-HT) have been determined in both the gas phase[6,7] and different solvents.[8] These species decay to the ground state (S_0) in less than 1 ps. Remarkably, the spectroscopic state S_2 decays within less than 100−150 fs to generate a longer lived transient species on the S_1 state. In jet experiments, *trans*-HT forms a S_1 transient with a ca. 250 fs lifetime,[7] while in solution, the lifetime is ca. 500 fs.[8]

The rationalization of these observations requires the detailed knowledge of the force field providing the driving force for the relaxation process. This force field can be conveniently discussed in terms of excited and ground state potential energy surfaces of the polyene. During the last few years significant progress in the computation of the excited states of *isolated* molecules has been achieved. In particular, it has been demonstrated that the excited state energetics of sizable polyenes (from butadiene to octatetraene) can be computed with reasonable accuracy by using high-level *ab initio* quantum chemical methodologies.[9] Most important, in a recent work we have demonstrated that computed excited state minimum energy paths (MEP) and reaction barriers for radiationless deactivation and *trans* → *cis* isomerization of a series of polyenes compare well with the available experimental data.[10]

In this report, high-level *ab initio* quantum chemical computations (MC-SCF[11a] and multireference Møller−Plesset perturbation theory[12a]) have been used to investigate the *composite*

[†] Università di Bologna.
[‡] King's College London.
[⊗] Abstract published in *Advance ACS Abstracts,* November 1, 1997.
(1) Zewail, A. H. *Femtochemistry*; World Scientific: Singapore, 1994; Vols. I and II.
(2) Zewail, A. H. *J. Phys. Chem.* **1996**, *100*, 12701−12724.
(3) (a) Leigh, W. J. In *CRC Handbook of Organic Photochemistry and Photobiology*; Horspool, W. M., Song, P.-S., Eds.; CRC Press: Boca Raton, FL, 1995; pp 123−142. (b) Laarhoven, W. H.; Jacob, H. J. C. ref 3a, pp 143−154. (c) Kohler, B. *Chem. Rev.* **1993**, *93*, 41.
(4) Petek, H.; Bell, A. J.; Christensen, R. L.; Yoshihara, K. *J. Chem. Phys.* **1992**, *96*, 2412.
(5) Hayden, C. C.; Chandler, D. W. *J. Phys. Chem.* **1995**, *99*, 7897−7903.
(6) Fuss, W.; Schikarski, T.; Schmid, W. E.; Trushin, S.; Kompa, K. L.; Hering, P. *J. Chem. Phys.* **1997**, *106*, 2205−2211.
(7) Cyr, D. R.; Hayden, C. C. *J. Chem. Phys.* **1996**, *104*, 771−774.
(8) Ohta, K.; Naitoh, Y.; Saitow, K.; Tominaga, K.; Hirota, N.; Yoshihara, K. *Chem. Phys. Lett.* **1996**, *256*, 629.
(9) Serrano-Andrés, L.; Lindh, R.; Roos, B. O.; Merchán, M. *J. Phys. Chem.* **1993**, *97*, 9360−9368.

S0002-7863(97)01280-8 CCC: $14.00

relaxation MEP of an isolated *trans*-HT molecule. This MEP has three sequential branches lying on the S_2, S_1, and S_0 potential energy surfaces with two distinct energy surface crossings (conical intersections)[13] that connect the S_2, S_1, and S_0 paths. The MEP provides information on the force field that the molecule "feels" on each state that, in turn, must ultimately determine the molecular dynamics. The structure of the S_2/S_1 and S_1/S_0 conical intersections provides information on the molecular deformation required to induce radiationless deactivation to the lower state. Thus in this work, the information on the reaction dynamics is obtained by investigating the structure of the force field which controls the *trans*-HT relaxation and isomerization processes. Quantum or semiclassical dynamics computations are not yet feasible for systems of this size.

In this paper we shall demonstrate that the computed *three-state* ($S_2 \rightarrow S_1 \rightarrow S_0$) relaxation path provides a mechanistic view of the ultrafast photochemistry of *trans*-HT, which is consistent with the experiment. The salient features of the reaction path are the following: (a) Motion out of the S_2 **FC** region and the subsequent relaxation along the S_1 energy surface lies within the space of *totally symmetric* deformations of the *trans*-HT molecular backbone. (b) The triggering of fast $S_1 \rightarrow S_0$ radiationless decay requires a *non-totally symmetric* deformation of the molecular backbone along a nearly barrierless (± 2 kcal mol^{-1}) path. (c) The molecular structure at the $S_1 \rightarrow S_0$ decay channel (i.e., at the S_1/S_0 crossing point) and its subsequent relaxation along the S_0 energy surface indicate that reactant back-formation must be the favored process. Thus our results (a and b) support the hypothesis that IVR (*internal vibrational energy redistribution*) from totally symmetric to non-totally symmetric modes must control the dynamics of ultrafast decay in short *all-trans* polyenes.

The excited state lifetime of linear polyenes increases dramatically when the polyene length is increased from hexatriene to octatetraene. Buta-1,3-diene and hexa-1,3,5-triene have both vanishingly small fluorescence yields[14] and very diffuse absorption spectra,[15] which is consistent with ultrafast excited state relaxation. In contrast, *all-trans*-octa-1,3,5,7-tetraene fluoresces from its first excited state (S_1) and has an excited state lifetime of several nanoseconds.[16] Thus, octatetraenes and longer polyenes do not show an ultrafast excited state relaxation dynamics. A comparison of the relaxation path computed for *trans*-HT to that of *s-trans*-butadiene and *all-trans*-octatetraene reveals that the magnitude of the barrier along the *asymmetric* deformation leading to $S_1 \rightarrow S_0$ radiationless decay fully accounts for the difference between "femtosecond" and "nanosecond" lifetime.

2. Computational Methods

All MC-SCF energy and gradient computations have been carried out with use of a complete active space (CAS-SCF) with double-ζ+ polarization (6-31G* and D95*) basis sets available in *Gaussian 94*.[11b] The effect of diffuse functions on geometry optimizations on the S_2 (ionic) potential energy surface has been tested by comparing the 6-31G* and 6-31+G* (i.e., a basis set with sp type diffuse functions on carbon atoms) energy differences and gradients on a few points. Since the two basis sets yield the same results, the 6-31G* basis set has been used for S_2 geometry optimization. All S_2, S_1, and S_0 minima, transition states, and MEPs have been computed using a 6 electrons in 6 orbitals active space (i.e., the six valence π orbitals) at the CAS-SCF level. To improve the energetics by including the effect of dynamic electron correlation, the energies have been re-computed by using multireference Møller−Plesset perturbation theory method, using the PT2F method[12a] included in *MOLCAS-3*.[12b]

The valence-ionic S_2 energy computations require some further elaboration. At the CAS-SCF level the order of B_u (valence-ionic) and B_u (Rydberg) is inverted with the B_u (Rydberg) coming lowest. When the PT2F energy is considered, the correct state ordering at the **FC** geometry is obtained (as observed by Roos and co-workers[17a]): B_u (valence-ionic) < $2A_g$ (valence-covalent) < Bu (Rydberg). Thus, the excitation energies and MEP energetics of the S_2 state have been evaluated by using the strategy indicated by Roos and co-workers.[17a] Accordingly, the Ag and Bu CAS-SCF reference wave functions required by PT2F computations are evaluated by using state averaged orbitals with the ANO basis set. In these cases the active space has been enlarged to 6 electrons in 8 orbitals (see footnote *c* in Table 1 for details) in order to be able to treat the possible intruder (Rydberg) states.[17] In conclusion, the S_2 minimum and MEP were "defined" by using CAS-SCF B_u (valence-ionic) *geometries* with PT2F *energies*. Similarly, the surface crossing between the B_u (valence-ionic) and the $2A_g$ covalent states are defined by computing the 2Ag PT2F energy at a few points along the S_2 MEP. We find that this crossing occurs very close to the **FC** geometry (within the first step of the S_2 MEP). One does need to demonstrate that the B_u (valence-ionic) surface at the CAS-SCF level has the correct shape even though it is obtained as an upper B_u state. This was confirmed by computing the 0−0 excitation energy and by generating data that can be directly compared with the Resonance Raman spectra. The S_2 minimum and MEP were first computed at the (Configuration Interaction Singles) CIS/6-31+G* level without symmetry constrains since this state is well represented at this level. These computations show that the minimum and the MEP can be obtained with C_{2h} symmetry. Accordingly, the S_2 MEP was computed at the CAS-SCF level, imposing C_{2h} symmetry by using both the 6-31G* and 6-31+G* basis set. While the two basis sets yield very similar coordinates, the MEP computation required state averaged orbitals (with 0.5 coefficients) to avoid root flipping between the lower and upper B_u states.

The *composite* $S_2 \rightarrow S_1 \rightarrow S_0$ *relaxation* path is computed in *four* steps. (i) In the first step we compute the MEP describing the S_2 relaxation from the **FC** region of our system. This MEP is unambiguously determined by using a new methodology[18] to locate the initial direction of relaxation (IRD) from the starting point (i.e. the *trans*-HT **FC** point). Briefly, an IRD corresponds to a local *steepest descent direction*, in *mass-weighted cartesians*, from a given starting point. The IRD is calculated by locating the energy minimum on a hyperspherical (i.e., $n-1$ dimensional) cross section of the n dimensional potential energy surface centred on the starting point (n is the number of vibrational degrees of freedom of the molecule). The radius of this hypersphere is usually chosen to be small (typically ca 0.25−0.5 au in *mass-weighted cartesians*) in order to locate the steepest direction in the vicinity of the starting point (i.e., the hypersphere center). The

(10) (a) Celani, P.; Garavelli, M.; Ottani, S.; Bernardi, F.; Robb, M. A.; Olivucci, M. *J. Am. Chem. Soc.* **1995**, *117*, 11584−11585. (b) Since the formation of the $-(CH)_3-$ kink involves the torsional deformation of two adjacent (one double and one single) bonds we believe that the S_1 motion in short polyenes can be described by the "Hula-twist" model proposed by Liu et al. (Liu, R. S. H.; Asato, A. E. *Proc. Natl. Acad. Sci. U.S.A.* **1985**, *82*, 259).

(11) (a) Roos, B. O. *Adv. Chem. Phys.* **1987**, *69*, 399−446. (b) The MC-SCF program we used is implemented in *Gaussian 94*, Revision B.2, M. J. Frisch, G. W. Trucks, H. B. Schlegel, P. M. W. Gill, B. G. Johnson, M. A. Robb, J. R. Cheeseman, T. Keith, G. A. Petersson, J. A. Montgomery, K. Raghavachari, M. A. Al-Laham, V. G. Zakrzewski, J. V. Ortiz, J. B. Foresman, C. Y. Peng, P. Y. Ayala, W. Chen, M. W. Wong, J. L. Andres, E. S. Replogle, R. Gomperts, R. L. Martin, D. J. Fox, J. S. Binkley, D. J. Defrees, J. Baker, J. P. Stewart, M. Head-Gordon, C. Gonzalez, and J. A. Pople, Gaussian, Inc.: Pittsburgh, PA, 1995.

(12) (a) Andersson, K.; Malmqvist, P-A.; Ross, B. O. *J. Chem. Phys.* **1992**, *96*, 1218. (b) *MOLCAS*, Version 3, K. Andersson, M. R. A. Blomberg, M. Fülscher, V. Kellö, R. Lindh, P.-A. Malmqvist, J. Noga, J. Olsen, B. O. Roos, A. J. Sadlej, P. E. M. Siegbahn, M. Urban, P. O. Widmark, University of Lund, Sweden, 1994.

(13) Bernardi, F.; Olivucci, M.; Robb, M. A. *Chem. Soc. Rev.* **1996**, *25*, 321−328.

(14) Myers, A. B.; Pranata, K. S. *J. Phys. Chem.* **1989**, *87*, 5079.

(15) Vaida, V. *Acc. Chem. Res.* **1986**, *19*, 114−120.

(16) (a) Kohler, B. E. *Chem. Rev.* **1993**, 93, 41−54. (b) Petek, H.; Bell, A. J.; Christensen, R. L.; Yoshihara, K. *SPIE* **1992**, *1638*, 345−356.

(17) (a) Serrano-Andrés, L.; Merchán, M.; Nebot-Gil, I.; Lindh, R.; Roos, B. O. *J. Chem. Phys.* **1993**, *98* 3151−3161. (b) See also: Serrano-Andrés, L.; Roos, B. O.; Merchán, M. *Theor. Chim. Acta* **1994**, *87*, 387.

(18) (a) Celani, P.; Robb, M. A.; Garavelli, M.; Bernardi F.; Olivucci, M. *Chem. Phys. Lett.* **1995**, *243*, 1−8. (b) Garavelli, M.; Celani, P.; Fato, M.; Bearpark, M. J.; Smith, B. R.; Olivucci, M.; Robb, M. A. *J. Phys. Chem.* **1997**, *101*, 2023−2032.

Table 1. Multireference Møller−Plesset Perturbation Theory (PT2F) and CAS-SCF (in parenthesis) Absolute (E) and Relative (ΔE) Energies for *trans*-HT[h]

structure	state	E (au)	ω[a]	ΔE (kcal mol^{-1})
S_0 **MIN (FC)**	S_0	−232.57108[b]	0.81	
		(−231.89131)		
		−232.74169[c]	0.79	
		(−231.97080)		
	S_1	−232.37632[b]	0.80	25.9[b]
		(−231.68227)		
		−232.55181[c]	0.76	
		(−231.76782)		
	S_2	(−231.61265[b])		
		−232.55547[c]	0.71	
		(−231.70289)		
S_2 **MIN**	S_1	−232.57848[c]	0.76	
		(−231.79882)		
	S_2	−232.55520[c]	0.72	
		(−231.71236)		
S_1 C_{2h}-**MIN**	S_0	−232.54399[b]	0.81	−79.4[b]
		(−231.85774)		
	S_1	−232.41752[b]	0.80	0.0[b]
		(−231.72735)		
		−232.51938[d]	0.80	0.0[d]
		(−231.75701)		
S_1 C_2-**MIN**	S_1	(−231.72740[b)]		
S_1 $\mathbf{TS_{E\rightarrow Z}}$	S_0	−232.47574[b]	0.80	−36.5[b]
		(−231.78621)		
	S_1	−232.41711[b]	0.80	0.3[b]
		(−231.71797)		
		−232.51944[d]	0.79	0.0[d]
		(−231.74849)		
S_2/S_1 **CI**	S_1	−232.55664[c]	0.72[c]	
		(−231.77367)		
	S_2	−232.55484[c]	0.68[c]	
		(−231.70511)		
S_1 **LP**[e]	S_0	−232.43771[b]	0.80	−12.7[b]
		(−231.74480)		
		(−231.73975)[b,f]		
	S_1	−232.41930[b]	0.80	−1.1[b]
		(−231.71957)		
		(−231.71518[b,f])		
S_1/S_0 **CI**[g]	S_0	(−231.71683[b,f])		
	S_1	(−231.71582[b,f])		
S_1 $\mathbf{TS_{t\rightarrow c}}$	S_1	−232.51653[d]	0.79	1.8[d]
		(−231.74997)		
S_1 $\mathbf{TS_{E\rightarrow Z\ adia}}$	S_1	−232.49055[d]	0.79	18.1[d]
		(−231.73063)		
S_1 $\mathbf{TS_{CH_2\ adia}}$	S_1	232.50773[d]	0.80	7.3[d]
		(−231.74692)		

[a] Weight of CAS-SCF reference function (i.e. the zeroth order function) in the first order function. [b] Structure and energy computed by using a 6 electrons in 6 orbitals CAS and the 6-31G* basis set. [c] Structure optimized by using a 6 electrons in 6 orbitals CAS and the 6-31G* basis set and energy computed by using symmetry adapted wave functions with a 6 electrons in 8 orbitals CAS, state averaged orbitals, and the ANO basis set C[6s,3p,1d], H[2s,1p] with a set of diffuse functions C[2p] on each carbon atom. The active space includes the 3 valence + 1 diffuse π-orbitals of Au symmetry and 3 valence + 1 diffuse π-orbitals of Bg symmetry. The state averaging includes the first three states of the chosen symmetry (either A_g or B_u) with 0.3333 weight each. [d] Structure and energy computed by using a 6 electrons in 6 orbitals CAS and the D95* basis set. [e] Last optimized point along the S_1 **MEP** (path III). [f] State averaged energy. The state averaging includes the first two states (S_0 and S_1) with 0.5 weight. [g] Optimized (lowest energy) crossing point. It is found that this point corresponds to the absolute energy minimum of the S_1 state. The corresponding structure is only slightly different from structure **LP** and <0.4 kcal mol^{-1} more stable. [h] The relative energies describe the energetics of the S_1 energy surface (see text for excitation energies).

IRD is then defined as the vector joining the starting point (i.e., the center of the hypersphere) to the energy minimum. Once one or more IRDs have been determined, the associated MEP is computed as *the steepest descent line in mass-weighted cartesians* by using the IRD vector to define the initial direction to follow. As we will discuss below, a planar and totally symmetric conical intersection structure (i.e., a S_2/S_1 real crossing) point has been located by simply following the resulting flat S_2 MEP until the S_2 and S_1 energies become degenerate. (ii) In the second step, we compute the MEP describing the S_1 relaxation processes from the totally symmetric S_2/S_1 conical intersection point (this is a highly unstable point, essentially a singularity, on the S_1 energy surface) determined in the first step. This second MEP is determined with the IRD method described above by choosing the S_2/S_1 intersection point as the starting point. Since this point is totally symmetric, the initial MEP direction has been located by using a fully asymmetric vector (generated via torsional deformation of the intersection structure) as the initial guess. The fact that the optimized vector corresponds to a totally symmetric displacement indicates that such displacement defines the bottom of a valley. Further, we find that the MEP ends at an energy minimum (i.e., a real intermediate) on the S_1 state. (iii) In the third step we compute the lowest lying reaction (non-totally symmetric) path describing the evolution of this S_1 intermediate. This S_1 MEP is computed in the conventional way by first locating a transition state on the non-totally symmetric path and running an intrinsic reaction coordinate computation in forward and reverse directions. We will see that this reaction path connects the totally symmetric intermediate with a non-totally symmetric S_1/S_0 conical intersection. (iv) Finally, in the fourth and last step we compute the S_0 MEPs describing two relaxation processes from the S_1/S_0 conical intersection using the IRD technique discussed above.

3. Results and Discussion

The total energies for all stationary points optimized on the S_2, S_1, and S_0 potential energy surfaces of *trans*-HT are reported in Table 1. The accuracy of the computed energy surfaces can be assessed *via* comparison with the experimental values for the vapor phase vertical and 0−0 excitation energies. Our computed values for the $1B_u$ and $2A_g$ vertical excitation energies at the PT2F level are 5.07 (experimental value 4.95 eV[19]) and 5.17 eV (experimental value 5.21[20]), respectively. These values also agree with the vertical excitation energies recently computed by Roos et al. using an experimental *trans*-HT molecular structure and the same ANO basis set.[17a] Our computed values for the 0−0 $1B_u$ and $2A_g$ excitation energy are 5.07 (experimental value 4.93 eV[21]) and 4.18 eV, respectively. While an experimental estimate for the 0−0 $2A_g$ excitation energy is lacking, this has been measured for the corresponding $2A_1$ state of *cis*-HT and is 4.26 eV.[22] The quality of the computed energy surfaces also has been assessed by comparison with the $1B_u$ (i.e., S_2) potential energy surface parameters derived via Resonance Raman (RR) spectroscopy. In Table 2 we show that the observed vapour phase S_0 frequencies and S_2 Δ_i factors[23] agree with the computed values.

In Figure 1 we give a schematic overview of our results. The *composite $S_2 \rightarrow S_1 \rightarrow S_0$ relaxation* path is represented by thick lines on the three potential energy sheets $\mathbf{S_2}$, $\mathbf{S_1}$, and $\mathbf{S_0}$. Equilibrium stationary points (S_2, S_1, and S_0 **MIN**) are represented by solid circles, transition states (S_1 **TS**) by open squares, and intersection points by open circles. The energy profile along the S_2 path (I in Figure 1) is flat and shows a S_2/S_1 crossing that occurs in the vicinity of the **FC** point. The S_1 path spans two different domains. The first domain (II in Figure 1) corresponds to a valley centered along a totally symmetric coordinate (see point ii in section 2) connecting the S_2/S_1 crossing point to the S_1 energy minimum (S_1 **MIN**). The

(19) Flicker, W. M.; Mosher, O. A.; Kuppermann, A. *Chem. Phys. Lett.* **1977**, *45*, 492.
(20) Fujii, T.; Kamata, A.; Shimizu, M.; Adachi, Y.; Maeda, S. *Chem. Phys. Lett.* **1985**, *115*, 369.
(21) Leopold, D. G.; Pendley, R. D.; Roebber, J. L.; Hemley, R. J.; Vaida, V. *J. Chem. Phys.* **1984**, *81*, 4218.
(22) Peteck, H.; Bell, A. J.; Christensen, R. L.; Yoshihara, K. *J. Chem. Phys.* **1992**, *96*, 2412.
(23) Ci, X.; Pereira, M. A.; Myers, A. B. *J. Chem. Phys.* **1990**, *92*, 4708−4717.
(24) (a) Orlandi, G.; Zerbetto, F.; Zgierski, M. Z. *Chem. Rev.* **1991**, *91*, 867. (b) Zerbetto, F.; Zgierski, M. Z. *J. Chem. Phys.* **1994**, *101*, 1842.

Table 2. CAS-SCF/6-31G* Ground State Vibrational Frequencies (ω_i) and $1B_2$ Displacement Parameters (Δ_i) for *trans*-HT Totally Symmetric Modes

ω_i (cm^{-1})		$\lvert\Delta_i\rvert$[d]			
calc[a]	exp[b]	grad[c]	geom[c]	exp[b]	assignment
332	354	93.5	48.1	19	skel bending
416	444	16.4	10.9	3.3	skel bending
907	934	19.3	25.9	3.4	CH_2 rocking
1166	1192	78.1	73.7	39	C−H bending
1264	1290	38.4	38.0	14	C−H bending
1286		5.6	6.3		C−H bending
1389	1403	21.4	14.1	0.4	CH_2 scissoring
1549	1581	0.35	4.9	8.8	skel stretching
1613	1635	100.0	100.0	100	skel stretching
2991		0.6	3.5		C−H stretching
2994		10.9	11.2		C−H stretching
3004		0.1	5.0		C−H stretching
3072		0.2	1.9		C−H stretching

[a] The ω_i values all have been multiplied by a 0.9 factor. [b] Data from ref 23. [c] The computed Δ_i factors have been determined according to two different treatments (see ref 24) from the S_2 energy gradient computed at the ground state *trans*-HT optimized structure (grad formulas) or from the geometrical displacements between the optimized S_2 and S_0 energy minima (geom formulas). [d] Notice that the most intense peak (Δ_{1635}) corresponds to the 1635 cm^{-1} stretch but, in general, the Δ_i/Δ_{1635} ratio is overestimated (especially in low-frequency modes and using the gradient (grad formulas). Nevertheless, the shape of the spectra is always reproduced.

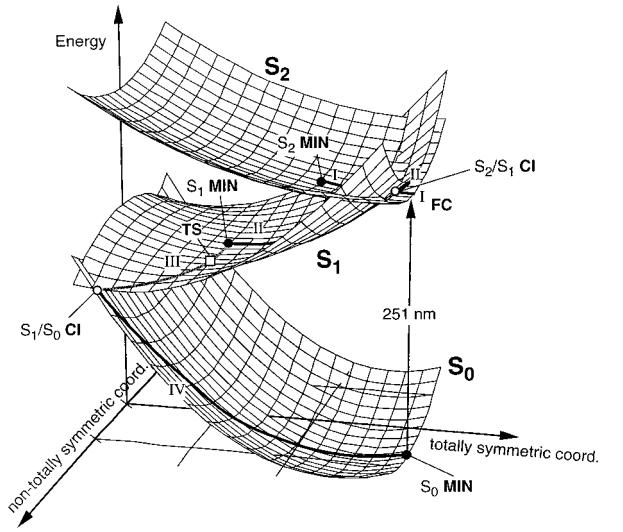

Figure 1. Three-dimensional representation of the S_0, S_1, and S_2 potential energy surfaces of *trans*-HT. The bold lines correspond to the computed relaxation/reaction paths (paths I, II, III, and IV) discussed in the text. The symbols (open circle, solid circle, and open square) and labels indicate the relevant stationary and crossing points located on the three energy sheets. Notice that on the S_1 sheet there are two paths: path II (solid line), which describes the S_1 relaxation process along a totally symmetric (C_{2h}) coordinate, and path III, which describes the nonadiabatic isomerization along a non-totally symmetric coordinate.

second domain (III in Figure 1) is defined by a fully asymmetric coordinate that connects the S_1 **MIN** to the S_1/S_0 crossing region through a transition structure (S_1 **TS**). This coordinate is dominated by torsional deformations, and it is therefore orthogonal to the coordinate describing the initial relaxation. Finally, the S_0 path (IV in Figure 1) connects the S_1/S_0 crossing to the original reactant potential energy well through a very steep and barrierless valley.

It is clear from Figure 1 that the spectroscopic state S_2 undergoes a very rapid depopulation due to the existence of a crossing in the vicinity of the **FC** point. This is consistent with the observed line width of the absorption and RR lines which indicates a lifetime near 40−50 fs.[25] The depopulation of S_2

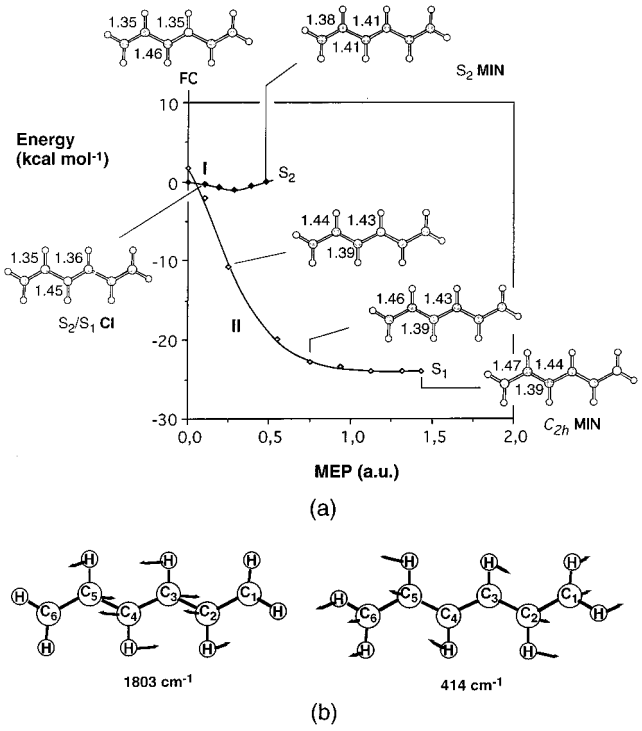

Figure 2. (a) Energy profiles along the two MEPs (path I and II) describing the relaxation from the **FC** and S_2/S_1 **CI** points. Solid and open diamond curves define the S_2 ($1B_u$) and S_1 ($2A_g$) branches of the *excited state* relaxation path, respectively. Because of the flatness of path I, the energy of all its points has been evaluated at the PT2F level. In contrast, the energy of all points in path II has been scaled to match the PT2F energies of the **FC**, S_2/S_1 **CI**, and C_{2h}-**MIN** (see Table 1). Notice that the PT2F correction yields a S_2 energy minimum, which is closer to the **FC** point with respect to S_2 **MIN**. The structures (geometrical parameters in Å and deg) document the geometrical progression along the relaxation path. (b) The shape of the high-frequency (1803 cm^{-1}) and low-frequency (414 cm^{-1}) C_{2h}-**MIN** totally symmetric modes describing the initial (steep) and final (flat) parts of the path II coordinate, respectively.

initiates a relaxation process that starts in the region of the S_2/S_1 crossing. The following subsections will describe the details of the relaxation paths sketched above. In particular, in subsection i we shall discuss the S_2 decay and the subsequent relaxation on the S_1 potential energy surface. In subsection ii the structure of the low-lying part of the S_1 potential energy surface will be documented. In subsection iii we will describe the relaxation and isomerization path in S_0, and finally in subsection iv we compare the structure of the S_1 potential energy surface for butadiene, hexatriene, and octatetraene.

(i) Depopulation of the Spectroscopic B_u (Valence-Ionic) State and Relaxation on S_1. In Figure 2a we show the computed MEP along the S_2 and S_1 potential energy surfaces. According to this diagram the depopulation of S_2 must be induced by a totally symmetric displacement toward the S_2/S_1 crossing, which involves simultaneous expansion of the double bonds and contraction of the single bonds. Notice that the S_2/S_1 crossing is located in the vicinity of the **FC** point and is accessed via "relaxation" toward the S_2 energy minimum. Due to the general flatness of the S_2 energy surface, the initial excited state motion out of the **FC** region is expected to be rather slow. For this reason it is very likely that after the $S_2 \rightarrow S_1$ decay the system merely accelerates along the initial part of the steep S_1 MEP (path II in Figures 1 and 2).

Along this S_1 MEP, the molecule conserves the C_{2h} symmetry and terminates at the stationary point C_{2h}-**MIN** located ca. 25

(25) Ci, X.; Myers, A. B. *J. Chem. Phys.* **1992**, *96*, 6433−6442.

kcal mol^{-1} below the **FC** point (and S_2/S_1 crossing). In general, the $S_2 \rightarrow S_1$ decay will not occur at exactly the crossing point but in its vicinity, including non-totally symmetric points. However, any path generated after the decay will be collected by the "totally symmetric" valley centered along path II. The C_{2h}-**MIN** structure shows the expected single/double bond inversion (the terminal and central double bonds expand by 0.12 and 0.09 Å, respectively, and the single bonds contract by 0.07 Å).

According to Table 1 and Figure 2a, an isolated S_1 *all-trans*-HT molecule has ca. 25 kcal mol^{-1} excess vibrational energy. Clearly, since path II lies within the space of totally symmetric vibrations, this energy would be *initially* concentrated in totally symmetric modes. If the S_1 energy surface was exactly quadratic, the molecular motion would indefinitely continue along these modes. In reality, non-totally symmetric vibrations will become populated because the surface is not quadratic. The population of non-totally symmetric vibrations initiates the process of IVR, where the excess energy will eventually be distributed to all the degrees of freedom of the system.

To establish if population of non-totally symmetric modes (and therefore IVR) is an essential prerequisite for radiationless decay to the ground state we have searched the totally symmetric coordinate subspace for the presence of a real crossing (i.e., conical intersection) between the S_1 and S_0 potential energy surfaces. Radiationless decay to the ground state, on a time scale shorter than IVR, will only occur in a region close to a S_1/S_0 conical intersection[26] or, in general, in a region where extremely efficient internal conversion (which usually involves small S_1-S_0 energy gaps) occurs. We have tried to locate and optimize a S_1/S_0 (under C_{2h} constraint) conical intersection; however, no energetically accessible (i.e., below the energy of the **FC** structure) conical intersection appears to exist in this C_{2h} subspace.

To provide further evidence that ultrafast internal conversion requires motion along non-totally symmetric modes, we have used the multidimensional separable harmonic surface model[27] to produce a 200 fs dynamics simulation of the excited state motion *on the totally symmetric subspace*. In fact, the shape of the energy profile (which changes from very steep to very shallow) and coordinate curvature (which increases in the region between 0.9 and 1.2 au) along path II (see Figure 2a) suggest that this MEP lies on the harmonic well defined by the totally symmetric vibrational modes of the C_{2h}-**MIN** S_1 minimum.[28] This is illustrated in Scheme 1, where we show that a path (i.e. steepest descent line) on a two-dimensional "model" harmonic well whose normal modes have very different frequencies has the same structural features of path II. Accordingly, we have generated a trajectory starting at the **FC** point with zero initial velocity. For each point generated (time step of 4 fs) we have computed the CAS-SCF/6-31G* energy. The results of this simulation are given in Figure 3 (see caption for computational details). It can be seen that the S_1-S_0 energy gap never falls below 65 kcal mol^{-1}, which is too large a gap for fast radiationless decay (experimentally determined $S_1 \rightarrow S_0$ internal conversion rate constants for aromatic hydrocarbons[29] give a 10^6-s^{-1} value for energy gaps near 60 kcal mol^{-1}). Therefore, we conclude that motion along the totally symmetric space is not compatible with ultrafast $S_1 \rightarrow S_0$ decay.

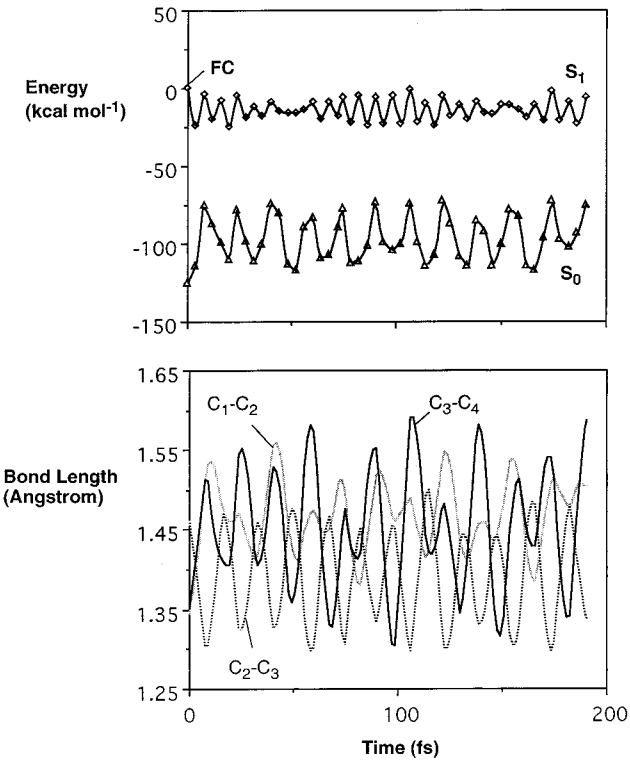

Figure 3. Time evolution of (top) the S_1 (open diamonds) and S_0 (open triangles) energies and (bottom) stretching parameters C_1-C_2, C_2-C_3, and C_3-C_4 (see Figure 2b for labels) during *all-trans*-hexatriene relaxation on the 13-dimensional totally symmetric cross section of the S_1 potential energy surface. The 200-fs trajectory has been computed within the approximation of the multidimensional separable harmonic surfaces by using eq 50 in ref 27 with a force field defined by computing the *ab initio* CAS-SCF/6-31G* vibrational frequencies at C_{2h}-**MIN**. The energies are relative to the simulation starting point **FC**.

Scheme 1

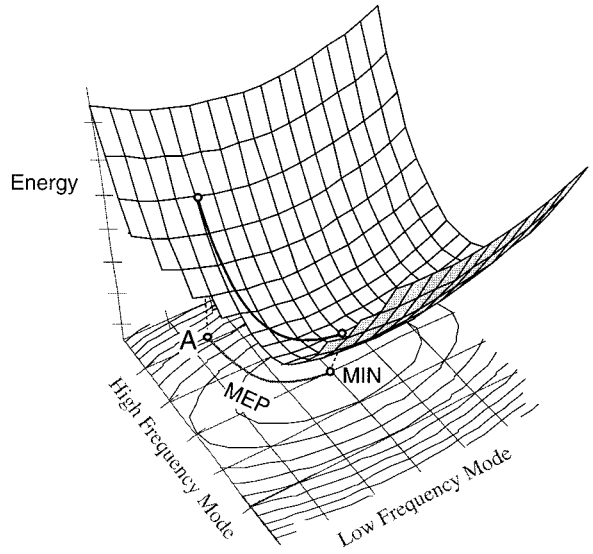

(ii) Structure of the Low-Lying Region of the S_1 Potential Energy Surface. Before we begin our discussion of the reaction pathways from the C_{2h}-**MIN** we need a brief aside on the nature

(26) See: (a) Yarkony, D. R. *Rev. Mod. Phys.* **1996**, *68*, 985−1013. (b) Yarkony, D. R. *J. Phys. Chem.* **1996**, *100*, 18612−18628.

(27) Myers, A. B.; Mathies, R. A. In *Biological Application of Raman Spectroscopy*; Spiro, T. G., Ed.; Wiley-Interscience: New York, 1987; Vol. 2, pp 1−58.

(28) More precisely, the projection of the initial mass-weighted displacement vector (i.e. computed at the beginning of path II) on the C_{2h}-**MIN** normal coordinates shows that the initial relaxation from the S_2/S_1 crossing is dominated by a single, high-frequency, mode that corresponds to the 1800 cm^{-1} stretch reported in Figure 2b. In contrast, the same vector computed along the terminal part of the same path has large components along low-frequency in-plane skeletal deformations such as the 414 cm^{-1} mode of Figure 2b. (There are other C_{2h}-**MIN** totally symmetric modes which have no negligible weights on the relaxation coordinate. These include a 1069 cm^{-1} stretching mode and a 1269 cm^{-1} in-plane C−H bending mode.)

(29) See for instance: Gilbert, A.; Baggott, J. *Essentials of Molecular Photochemistry*; Blackwell Scientific Publications: Oxford, 1991.

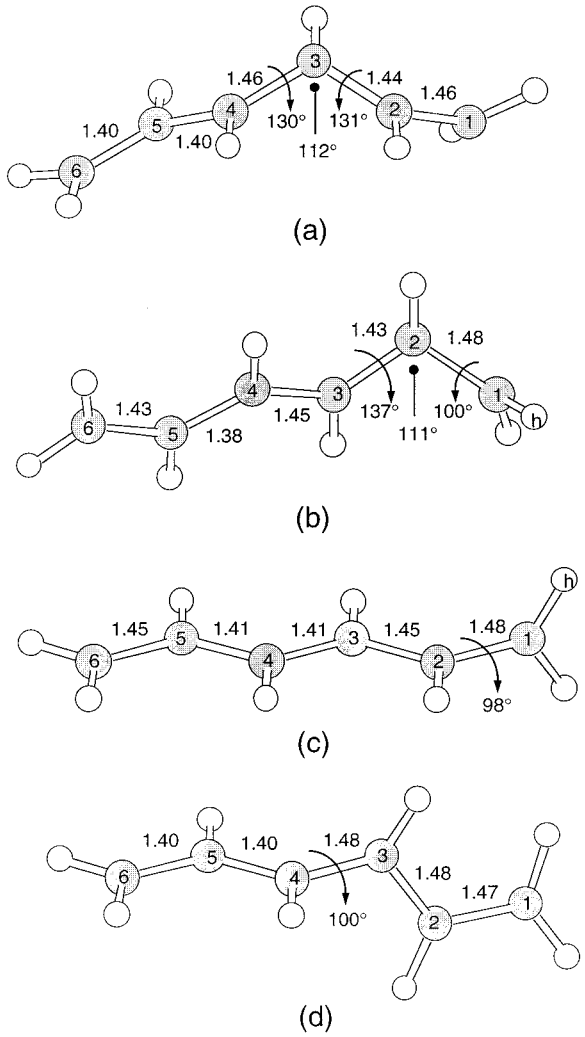

Figure 4. Molecular structure and relevant geometrical parameters (Å and deg) for the S_1 low-lying transition structures (see text) in order of increasing energy: (a) $\mathbf{TS_{E\rightarrow Z}}$, (b) $\mathbf{TS_{t\rightarrow c}}$, (c) $\mathbf{TS_{CH_2\ adia}}$, and (d) $\mathbf{TS_{E\rightarrow Z\ adia}}$.

of the surface in the immediate vicinity of this minimum. At the CAS-SCF/6-31G* level, the C_{2h}-**MIN** has two low imaginary frequencies (143 i and 118 i cm^{-1}) corresponding to a conrotatory (e.g., clockwise, clockwise) and disrotatory (e.g., clockwise, counterclockwise) torsion of the two terminal CH_2 groups. The 143 i cm^{-1} mode leads to an equilibrium stationary point (lowest frequency 88 cm^{-1}) of C_2 symmetry (S_1 C_2-**MIN**), which is <0.1 kcal mol^{-1} below that of S_1 C_{2h}-**MIN** (see Table 1). Thus one must regard the *trans*-HT equilibrium C_{2h}-**MIN** structure as having essentially free rotating CH_2.

The *lowest-lying* region of the S_1 potential energy surface starts at the C_{2h}-**MIN** energy minima and develops along non-totally symmetric coordinates. We have located two non-adiabatic $\mathbf{TS_{E\rightarrow Z}}$ (Figure 4a) and $\mathbf{TS_{t\rightarrow c}}$ (Figure 4b), and two adiabatic, $\mathbf{TS_{CH2\ adia}}$ and $\mathbf{TS_{E\rightarrow Z\ adia}}$, "*cis-trans*" isomerization paths defined by the four transition structures given in Figure 4.

The non-adiabatic transition structures $\mathbf{TS_{E\rightarrow Z}}$ (Figure 4a) and $\mathbf{TS_{t\rightarrow c}}$ (Figure 4b) are characterized by the presence of a well-developed "kink", which involves the $C_2-C_3-C_4$ and $C_1-C_2-C_3$ angles in $\mathbf{TS_{E\rightarrow Z}}$ and $\mathbf{TS_{t\rightarrow c}}$, respectively. This "$-(CH)_3-$" kink has been documented before[10] for a series of six linear polyenes (i.e., from allyl radical to octatetraene), and the reaction paths via the corresponding transition states lead to a conical intersection between the S_1 and S_0 potential energy surface. Such intersections form extremely efficient radiationless deactivation channels.[26] $\mathbf{TS_{E\rightarrow Z}}$ is associated with a *non-adiabatic* (i.e., the isomerization motion involves two different energy surfaces) E → Z (because of the large ca. 50° torsion about the central double bond) isomerization and $\mathbf{TS_{t\rightarrow c}}$ with a *non-adiabatic* single-bond (i.e., t → c) isomerization (because of the 43° torsion about the single-bond). The $\mathbf{TS_{E\rightarrow Z}}$ transition state and isomerization paths will be discussed in detail in the next subsection.

The adiabatic transition structures $\mathbf{TS_{CH_2\ adia}}$ and $\mathbf{TS_{E\rightarrow Z\ adia}}$ define two isomerization paths on the excited state connecting the *all-trans* S_1 **MIN** structure to itself (via a 180° rotation of one terminal CH_2 group) and connecting the *cis*-HT structure (via a 180° *trans* → *cis* rotation about the central C═C bond), respectively. In Figure 4, parts c and d, we show that these structures show a ca. 90° twisted double bond and thus lie halfway along the S_1 isomerization path.

The energy barriers controlling the access to the four isomerization paths described above are given in Table 1. It is remarkable that the adiabatic paths have larger barriers. Indeed the lowest adiabatic reactive process, which corresponds to CH_2 rotation, has a ca. 7 kcal mol^{-1} barrier. Both non-adiabatic paths (i.e. $\mathbf{TS_{E\rightarrow Z}}$ and $\mathbf{TS_{t\rightarrow c}}$) are energetically favored, and the path associated with E → Z motion is nearly barrierless. The same type of potential energy surface topology has been recently documented for the S_1 excited state of *all-trans*-octatetraene.[30]

(iii) S_1 → S_0 Radiationless Decay and Trans → Cis Isomerization. To gain insight into the mechanism of the S_1 → S_0 radiationless decay and photochemical *trans* → *cis* isomerization we have investigated the structure of the energy surface along the reaction valley defined by the lowest lying S_1 transition structure ($\mathbf{TS_{E\rightarrow Z}}$). In Figure 5 we have reported the energy profile and geometrical evolution along the computed MEP (path III). As already mentioned above, this path leads to a S_1/S_0 conical intersection. The MEP stops at a point (labeled S_1 **LP** in Figure 5) where the energy separation between the S_1 and ground state is only ca. 10 kcal mol^{-1}. A conical intersection optimization starting from this point yields a similar structure (S_1/S_0 **CI**) where the S_1 and S_0 energies are degenerate (see Table 1). The flatness of path III and the molecular geometries in Figure 5 suggest that this deformation will be prompted by population of very low frequency and non-totally symmetric modes of C_{2h}-**MIN**.

The mechanism for ground state relaxation occurring just after S_1 → S_0 decay was investigated by searching for all possible S_0 valleys in the region around the crossing point. (See the computational details section and ref 18b for a previous application.) In Figure 5 we show that there are two such valleys. The first valley (path IV in Figure 5) leads to ground state *all-trans*-HT and is therefore associated with the reactant back formation process. The second valley (path V) is associated with the reactant *trans* → *cis* isomerization process. The last structure reported in Figure 5 has a 2° central torsional angle consistent with a fully isomerized central double bond. However, also notice that one of the adjacent single bond has undergone a large rotation, featuring a 56° torsional angle. This means that path V describes a process of simultaneous double-bond (E → Z) and single-bond (t → c) isomerization leading to *tZc*-HT as the primary photoproduct.

The quantum yield of the *trans*-HT isomerization is given by the percent of excited state molecules that, after decay, relax along the valley defined by path V. The quantitative evaluation of this quantity requires dynamic treatment of the non-adiabatic motion on the S_1 and S_0 potential energy surfaces. However, our data allow us a few qualitative considerations. The structure of the S_2 and S_1 energy surfaces indicates that S_1 and S_0 decay is prompted by IVR from totally symmetric to non-totally

(30) Garavelli, M.; Celani, P.; Yamamoto, N.; Bernardi, F.; Robb, M. A.; Olivucci, M. *J. Am. Chem. Soc.* **1996**, *118*, 11656−11657.

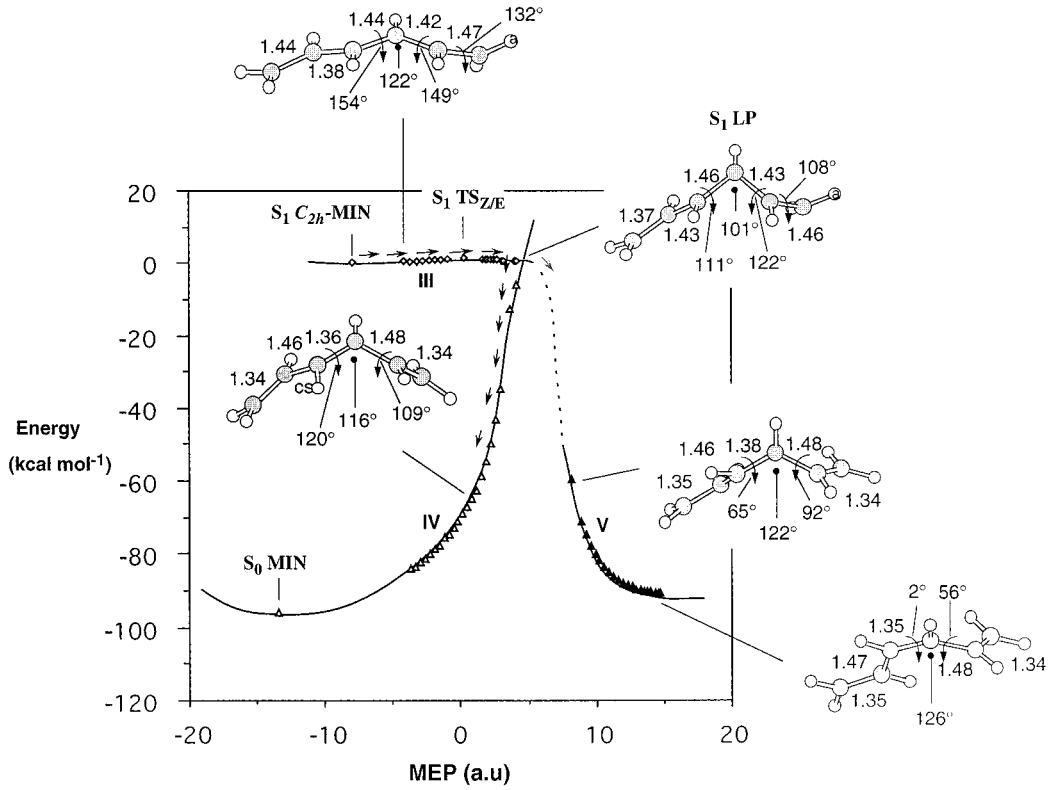

Figure 5. Energy profiles along the three MEPs describing the $S_1 \rightarrow S_0$ decay, S_0 relaxation, and photoproduct formation from C_{2h}-**MIN**. The open diamond curve defines the S_1 ($2A_g$) lowest-lying reaction path (path III). The open triangle and solid triangle curves define the S_0 concurrent *ground state* paths leading to reactant back formation (path IV) and *trans* → *cis* isomerization (path V). The energies of all points have been scaled to match the PT2F energies of the C_{2h}-**MIN**, **TS**$_{Z/E}$, S_1 **LP** and **FC** (see Table 1). The structures (geometrical parameters in Å and deg) document the geometrical progression along the relaxation paths.

Scheme 2

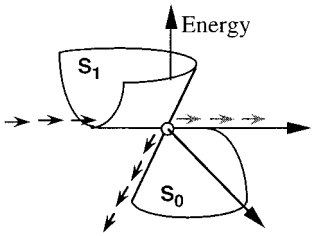

symmetric modes. Since ca. 25 kcal mol^{-1} of vibrational excess energy will be distributed among 36 degrees of freedom, we expect that the average velocity of the system along the flat path III will be small. Under these conditions, the structure of the S_0 potential energy surface in the vicinity of the decay point does provide an indication of the population of the ground state valleys IV and V. The energy profiles in the vicinity of the **LP** point (see Figure 5) indicate the presence of a "tilted" conical intersection of the type illustrated in Scheme 2 (this is also called an intermediate[31] intersection). Indeed, several attempts to locate, in the vicinity of the crossing, an IRD pointing in the direction of path V have failed. The computations indicate that this valley only starts to exist at a much larger (4.0 au) distance than the IRD pointing along path IV. Thus a system that is moving with *low* velocity in the direction of the tip of the cone and hops to S_0 *in the vicinity* of the tip will preferentially populate the reactant back formation valley. Only a small number of S_1 molecules will have enough kinetic energy to reach the *trans* → *cis* isomerization valley. This seems to be consistent with the observed 0.016[32] quantum yield for *trans* → *cis* photoisomerization in solution.

(iv) S_1 Radiationless Decay Paths in Shorter and Longer Trans Polyenes. Buta-1,3-diene and hexa-1,3,5-triene have vanishingly small fluorescence yields.[15] Further, their absorption spectra are very diffuse even at low temperatures. These facts indicate that these molecules have very short excited state lifetimes. This behavior is in contrast with that of octa-1,3,5,7-tetraene (and longer polyenes), which fluoresces from its first excited state (S_1) and has an excited state lifetime of several nanoseconds.[16] In the preceding subsections we have demonstrated that, in *trans*-HT, the fast radiationless decay is triggered by molecular distortion along a flat valley (path III) leading to a S_1/S_0 conical intersection. This result suggests that the S_1 lifetime in shorter and longer *all-trans* polyenes is mainly controlled by the structure of the paths connecting the S_1 C_{2h} stationary point to the lowest lying, strongly asymmetric, S_1/S_0 conical intersection. The energy profiles along the S_1 branch of such non-adiabatic isomerization paths are given in Figure 6 for the three polyenes mentioned above. The longer polyene, *all-trans*-octatetraene, is the only one with a non-negligible (ca. 7.5 kcal mol^{-1}) barrier located along the reaction path. For this reason we expect this molecule to have a non-negligible S_1 lifetime, consistent with the experiment. As seen in subsection iii, *trans*-HT has a much smaller (ca. 0 kcal mol^{-1}) barrier and can therefore undergo a rapid (subpicosecond) decay to the ground state. Finally, in *s-trans*-butadiene the barrier becomes largely negative (notice that, from the topological point of view, the marked and very shallow energy maxima located along the octatetraene and hexatriene energy profiles correspond to an inflection point in butadiene). Butadiene must therefore have a lifetime probably shorter than that of *trans*-HT.

(31) Atchity, G. J.; Xantheas, S. S.; Ruedenberg, K. *J. Chem. Phys.* **1991**, *95*, 1862−1876.

(32) (a) Jacobs, H. J. C.; Havinga, E. *Adv. Photochem.* **1979**, *11*, 305. (b) Vroegop, P. J.; Lugtenburg, J.; Havinga, E. *Tetrahedron* **1973**, *29*, 1393.

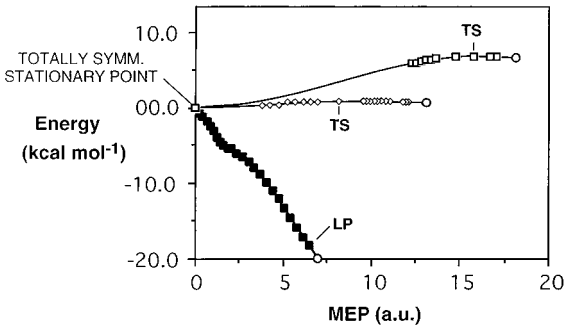

Figure 6. Energy profiles along the three MEPs describing the $S_1 \rightarrow S_0$ decay process of the S_1 C_{2h} stationary points of three *all-trans* polyenes. The solid square curve defines the S_1 ($2A_g$) lowest-lying reaction path in *s-trans*-butadiene.[10] The open diamond curve defines the S_1 ($2A_g$) lowest-lying reaction path (path III in this paper). The open square curve defines the S_1 ($2A_g$) lowest-lying reaction path in *all-trans*-octatetraene.[30] Open circles indicate conical intersection points. The energies of all points have been scaled to match the PT2F energies of the stationary points, including the totally symmetric minima, the two transition states (**TS**), and the last MEP point (**LP**) indicated in the figure.

Scheme 3

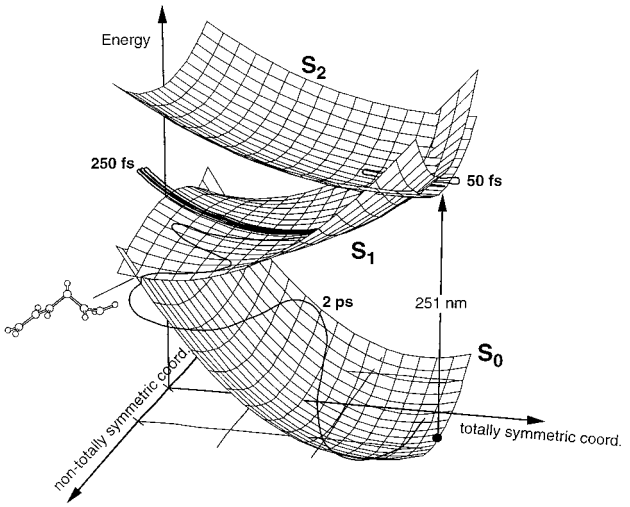

4. Conclusions

In this paper we have documented the reaction path for the evolution of a molecular structure along a *three-state* ($S_2 \rightarrow S_1 \rightarrow S_0$) photochemical pathway for *trans*-HT using a method to locate and follow the energy valleys (IRD) which develop from the **FC** point and from two different conical intersection points (S_2/S_1 **CI** and S_1/S_0 **CI**). This path can be used to derive a *qualitative* view (summarized in Scheme 3) of the excited state dynamics prompted by a 0−0 transition (i.e., in a condition where the photoexcited reactant has little initial vibrational excess energy). In this scheme the trajectory of a *trans*-HT molecule (or vibrational wavepacket) is represented by a solid line on the potential energy surfaces of Figure 1. As mentioned in the introduction, the ultrafast *trans*-HT dynamics following 0−0 excitation to the S_2 state recently have been experimentally investigated by Hayden[7] and Yoshihara[8] using different methodologies. These authors reach the same conclusion that the S_2 depopulation must be extremely fast (<100 fs), consistent with the 40 fs time scale previously estimated on the basis of Resonance Raman line shape analysis.[14] Remarkably, our computations suggest that while the system *slowly* accelerates along the flat S_2 energy surface, ultrafast internal conversion to S_1 must take place via the S_2/S_1 **CI** channel at a *planar* C_{2h} geometry not much different from that of the **FC** point (see Figure 2a for details). The prediction that $S_2 \rightarrow S_1$ decay occurs via totally symmetric displacements is consistent with the experimental data reported by Hayden et al., who exclude torsional excitation induced by $S_2 \rightarrow S_1$ decay.[7] Furthermore, Fuss et al. have recently reported[33] that the S_1 ($2A_1$) transient absorption spectra of *cis*-HT (generated via excitation to the S_2 ($1B_2$) state of this molecule) is different from that of *trans*-HT, demonstrating that these isomers do not undergo S_2 or S_1 *cis* $\rightarrow$ *trans* interconvertion.

According to Scheme 3, the initial motion on the S_1 energy surface occurs only along C_{2h} displacements. This result is consistent with the experimental data reported by Hayden et al., who exclude torsional excitation induced by the $S_2 \rightarrow S_1$ decay process[7]. These authors observe that independently generated S_1 *trans*- and *cis*-HT isomers do not interconvert during the S_1 lifetime. Our computations show that while an S_1 *trans*-HT molecule has enough excess energy (ca. 25 kcal mol^{-1}) to overcome the computed *trans* $\rightarrow$ *cis* isomerization barrier at $\mathbf{TS_{E\rightarrow Z\ adia}}$, this energy is concentrated in totally symmetric modes of the type shown in Figure 2b. The conjecture (Scheme 3 and Figure 3) that this energy remains trapped on such modes until it is redistributed among all degrees of freedom has also been experimentally tested. In fact, Yoshihara et al.[8] have provided experimental evidence that the depopulation of vibrationally hot S_1 states in *trans*-HT cannot occur via enhanced fast internal conversion from these states but only via IVR on the S_1 energy surface itself. We take this observation as experimental evidence of the lack of an accessible S_1/S_0 conical intersection along the totally symmetric subspace as described in subsection i.

While the quantitative evaluation of the time scale for IVR is beyond the scope of this work, the existence of a S_1/S_0 conical intersection located along a very flat S_1 valley (see Figure 5) suggests that the time scale for $S_1 \rightarrow S_0$ cannot be much larger than the time required for IVR. Thus as suggested in Scheme 3 we expect that efficient and fast internal conversion will take place soon after IVR has filled the first torsional levels of the S_1 **MIN** structure. This process will ultimately result in the geometrical deformation leading to the documented[10] $-(CH)_3-$ kinked intersection. Therefore, our results reinforce the experimental interpretation: the observed 250-fs lifetime of gas-phase *trans*-HT must correspond to the time required for IVR.

Acknowledgment. We are grateful to Werner Fuss for reading the original manuscript and for many helpful comments. This research has been supported in part by the EPSRC (UK) under Grant No. GR/K04811, by an EU TMR network grant (ERB 4061 PL95 1290, Quantum Chemistry for the Excited State), and by the "Access to Supercomputing Facilities for European Researchers" project of the Training and Mobility of Researchers (contract ERBFMGECT950062 (DG-12 MEMO)) established between the European Community and CESCA/CEPBA. We are also grateful to NATO for a travel grant (CRG 950748).

Supporting Information Available: Listing of Cartesian co-ordinates of all structures reported in Table 1 (4 pages). See any current masthead page for ordering and Internet access instructions.

JA971280U

(33) Lochbrunner, S.; Fuss, W.; Kompa, K. L.; Schmid, W. E. *Chem. Phys. Lett.* **1997**, *274*, 491−498.